



HAL
open science

A classical molecular dynamics simulation method for the formation of “dry” gels from boro-aluminosilicate glass structures

Mélanie Taron, Jean-Marc Delaye, Stéphane Gin

► **To cite this version:**

Mélanie Taron, Jean-Marc Delaye, Stéphane Gin. A classical molecular dynamics simulation method for the formation of “dry” gels from boro-aluminosilicate glass structures. *Journal of Non-Crystalline Solids*, 2021, 553 (1), pp.120513. 10.1016/j.jnoncrysol.2020.120513 . cea-04737588

HAL Id: cea-04737588

<https://cea.hal.science/cea-04737588v1>

Submitted on 13 Nov 2024

HAL is a multi-disciplinary open access archive for the deposit and dissemination of scientific research documents, whether they are published or not. The documents may come from teaching and research institutions in France or abroad, or from public or private research centers.

L'archive ouverte pluridisciplinaire **HAL**, est destinée au dépôt et à la diffusion de documents scientifiques de niveau recherche, publiés ou non, émanant des établissements d'enseignement et de recherche français ou étrangers, des laboratoires publics ou privés.



Distributed under a Creative Commons Attribution - NonCommercial 4.0 International License

A classical molecular dynamics simulation method for the formation of “dry” gels from boro-aluminosilicate glass structures

Mélanie Taron, Jean-Marc Delaye, Stéphane Gin

CEA, DES, ISEC, DE2D, University of Montpellier, Marcoule, F-30207 Bagnols-sur-Cèze, France

Abstract

In contact with water, glass transforms into amorphous and porous structures called gels. A simulation method based on classical molecular dynamics is proposed here to mimic “dry” gels forming from initial oxide glass structures. Six glass compositions were investigated. Two behaviours were **evidenced** depending on the initial glass composition, and in particular on the quantity of elements removed. If a large quantity of soluble elements (B, Na) was removed, it induced an increase in the average pore size within the gels, and the time needed to **stabilise** the gel structure increased because more local atomic rearrangements occurred. The gel network displayed a higher proportion of Si-Q₄ at the expense of Si-Q₃ and a lower average ring size compared to the glass network, irrespective of the glass composition. Surface effects were also highlighted in the dry gels, such as the presence of 3-coordinated Al and a decrease in the average angle **Si-O-Si and Al-O-Al**. These findings will be compared to both wet gels and experimental data in further studies, to help find the best procedure to simulate such structures.

Introduction

Borosilicate glasses are of great technological interest because of their versatility and the various properties they offer¹. One of their many applications is found in the nuclear field, where they are used to contain high-level radioactive wastes from spent nuclear fuel reprocessing. After cooling for a few decades, the vitrified wastes will be stored in a deep geological repository². To prepare for this, many studies have been performed on glass durability in order to assess the safety of such a disposal system over a geological time scale²⁻⁵. It has been observed that when in contact with water, glass dissolves firstly at an initial rate, then decreasingly through time until it reaches a rate several orders of magnitude lower, called the residual rate². This decrease has been attributed to the formation of a passivating alteration layer, usually referred to as gel^{6,7}.

The gel is **characterised** by its porous, amorphous, and hydrated structure. Depending on its open porosity, it can act as a diffusion barrier for aqueous species^{8,9}. The mechanisms behind the formation of such a gel have been widely discussed, resulting in two main theories: the gel may be defined as a “residual” glass skeleton depleted in soluble elements such as alkali and boron^{8,10}, or on the other hand, it may be the result of the precipitation of dissolved species at the interface with the altering solution^{11,12}. However, neither approach necessarily excludes the other.

To date, there no consensus has been reached as to the origin of the passivating effect of gels, which thus remains an open question. Studies have suggested that it may originate from their ability to act as a barrier to both water and reaction product diffusion, thus limiting the dissolution process by

40 partially sealing diffusive canals^{13,14}. Another explanation, proposed by Du et al.¹⁵, suggests an
41 increase in the number of small silicate rings within the gels resulting in a decrease in water mobility.

42 However, it appears that the passivating properties of the gel greatly rely on several factors, such as
43 the glass composition^{14,16} and the altering solution composition (pH^{17,18}, concentration of ions¹⁹⁻²²).
44 Consequently, it is also important to underline that the morphology of the gel also changes over time
45 due to a maturation process²³ and the incorporation of exogenous elements^{20,21}, making it even
46 harder to ascribe the passivation to one definitive mechanism. Several studies have investigated gel
47 morphologies. For example, it has been shown that the size of the pores depends on the pH of the
48 solution, as higher pH levels lead to an increasing porosity due to the higher solubility of silicon²⁴.
49 Moreover, a gel morphology can display open and/or closed pores¹³, as well as an uneven pore
50 distribution through the gel layer, which can appear to be denser at the interface with the solution²⁴.
51 Many studies have been conducted on the impact of the glass composition on gel properties, by both
52 experimental approaches and Monte-Carlo simulations^{16,25-27}. While these have highlighted the role
53 of specific elements such as Al²⁷, to date no global model has emerged to enable a better
54 understanding of the link between glass composition and gel properties. **In this study we focused on**
55 **six glasses and gels of various compositions by classical molecular dynamics.** This two-part study is
56 attempting to link both the structure and the composition of gels to various properties of the
57 passivating layer.

58 Classical molecular dynamics simulations have proven to be an invaluable tool in probing the
59 structure of glasses^{10,28-30} and gels^{31,32} at both short and medium range order. Several methods exist
60 to simulate gels, from the removal of blocks of silicon atoms to simulate an ordered porosity^{33,34}, to
61 the introduction of defects using **hydrogarnet** defects³² or modification of the simulation parameters,
62 for example like charge scaling, mimicking a sol-gel process³⁵, and volume scaling^{36,37}. However, it has
63 not yet been possible to directly reproduce the experimental mechanisms leading to the formation of
64 the gel with water. Classical molecular dynamics were therefore used here to study six simulated
65 “dry” (without water) gels. The gels were obtained from five-oxide (Si-Al-B-Na-Ca) glasses and then
66 depleted in soluble elements, with the exception of calcium which has already been proven to be
67 retained in the gel layer^{10,38}. The gels were annealed in order to simulate their **stabilisation** with time,
68 enabling a continuous, dynamic structural analysis. Comparisons between the gels and their
69 respective glasses will give an indication of the impact of the initial glass composition on the
70 structure and morphology of the gel. This paper details the first part of a longer study intended to
71 simulate wet gels by introducing water into the porous volumes of the dry gels described here. These
72 wet gel properties will be presented in a second article.

73 **Methods**

74 **Glass compositions**

75

	Composition (mol%)					S/I	SiO ₂ /Al ₂ O ₃	Density ³⁹ (g/cm ³)	T (K)
	SiO ₂	B ₂ O ₃	Al ₂ O ₃	CaO	Na ₂ O				
S65.5	65.50	9.00	6.84	6.00	12.66	0.3	9.6	2.49	3400
S57.5	57.50	18.00	5.84	6.00	12.66	0.6	9.8	2.44	3000
S51.0	51.00	22.00	5.34	6.00	12.66	0.9	9.6	2.34	3400
S52.5	52.50	19.00	9.84	6.00	12.66	0.6	5.3	2.36	3200
S57.5	57.50	18.00	5.84	6.00	12.66	0.6	9.8	2.44	3000

S63.0	63.00	17.00	1.34	6.00	12.66	0.6	47.0	2.48	3000
CJ3	61.16	16.29	3.89	5.81	12.85	0.6	15.7	2.47	3200

Table 1 – Composition, soluble / insoluble ratio (S/I), SiO₂/Al₂O₃ ratio, density and maximum simulated temperature T of the studied glasses

76
77

78 Six five-oxide glasses divided into two series were designed in order to assess the impact of two
79 particular ratios (the ratio between soluble and insoluble elements, S/I, and the SiO₂/Al₂O₃ ratio) on
80 the structure and properties of the resulting simulated gels. The compositions are given in Table 1. In
81 the first series, composed of S65.5, S57.5, and S51.0, the SiO₂/Al₂O₃ ratio remained constant with
82 only the S/I ratio varying. Inversely, with a varying SiO₂/Al₂O₃ ratio and constant S/I ratio, the second
83 series was composed of S52.5, S63.0, and S57.5, to which was added CJ3 which has been studied
84 elsewhere and meets the necessary criteria⁴⁰.

85 In order to define the soluble and insoluble elements, the following assumptions were made based
86 on previous studies, either by MD or experiments^{10,38}:

- 87 - Soluble elements are B, Ca, and the quantity of Na associated with non-bridging oxygen (H1)
- 88 - Insoluble elements are Si and Al (H2)
- 89 - **Four fold-coordinated Al⁴** is compensated before **four fold-coordinated B⁴**, and firstly by Na,
90 then Ca (H3)
- 91 - **B⁴** is compensated by Na (H4).

92 For instance, using S52.5 as an example, the S/I calculation is as follows: from (H3), the Al quantity is
93 inferior to the Na quantity, meaning that all Al are compensated by Na. From (H4) and (H3), the
94 quantity of B compensated by Na is the remaining quantity of Na that does not compensate Al. The
95 4-fold coordinated B quantity is therefore (Na₂O₃ - Al₂O₃): all Na are charge compensators and there
96 are no Na associated with non-bridging oxygens. Thus, from (H1), the soluble elements correspond to
97 the Ca and B atoms, i.e. CaO + 2*B₂O₃. The insoluble elements are, from (H2), the quantity of Si and
98 Al, i.e. SiO₂ + 2*Al₂O₃.

99 Simulation of the glasses

100 Glasses were prepared using the LAMMPS code⁴¹ with potentials (Coulomb - Buckingham type)
101 developed by Du et al²⁸ (see Supplementary Information Table S1 and Table S2) following Equation
102 (1), taking into account two-body potentials at short range (a repulsive exponential term and an
103 attractive dipolar term) and long-range Coulombic interactions:

$$V_{ij} = A_{ij}e^{-\frac{r_{ij}}{\rho_{ij}}} - \frac{C_{ij}}{r_{ij}^6} + \frac{q_i q_j}{r_{ij}} \quad (1)$$

104 where *i* and *j* are the atoms of the *i-j* pair, *A_{ij}*, *ρ_{ij}* and *C_{ij}* are the short range pair potential parameters,
105 *r_{ij}* the interatomic distance between the atoms *i* and *j*, and *q_i* and *q_j* are the partial charges for the
106 atoms *i* and *j*. A repulsive term described in Equation (2) was added to overcome strong attractions
107 at small interatomic distances induced by the Buckingham potential:

$$V_{ij}(r_{ij}) = \frac{B_{ij}}{r_{ij}^{n_{ij}}} + D_{ij}r_{ij}^2 \quad (2)$$

108 where *B_{ij}*, *n_{ij}* and *D_{ij}* are parameters fitted to allow continuity in the potential, the force, and the first
109 derivate of the force at the distance where the second derivate of the force is close to zero.

110 The simulated systems were composed of 100 000 randomly generated atoms, for which the box size
111 was determined with respect to the estimated density of each glass based on Fluegel's work³⁹. Long-
112 range interactions were computed with a **Particle-Particle-Particle-Mesh** (PPPM) algorithm, with a
113 defined accuracy of 10⁻⁵. The cut-off used for the short-range interaction was 10 Å. All simulations

114 were performed with a 1 fs time step. A first equilibration step was performed at 1000 K for 0.1 ps in
115 the NVT ensemble (constant number of atoms, volume, and temperature) to remove the initial most
116 energetic interactions. The structure thus obtained was then heated to 3000 K < T < 3400 K for 1 ns
117 (NVT ensemble) in order to lose the memory of the initial configuration, and quenched at a 2 K/ps
118 rate to 300 K in the NVT ensemble. Afterward, two successive 20 ps equilibration steps were
119 performed, firstly in the NVT ensemble, then in the NVE ensemble (constant number of atoms,
120 volume, and energy).

121 Formation of the gels

122 Gels were obtained from the simulated glass by removing all boron atoms as well as all sodium, with
123 the exception of two gels (S65.5 and S52.5). For these, part of the sodium was used to compensate
124 aluminium and thus it was left in the gel. In order to maintain the electro-neutrality of the system, it
125 was necessary to remove some oxygen atoms. They were selected randomly from the boron and
126 sodium first-neighbour environments. Once prepared, the new system was equilibrated for 0.5 ns in
127 the NVT at 300 K ensemble before being heated to 2400 K in the same conditions. This step was
128 conducted for 0.5 ns, and enabled the gel structure to be annealed and stabilised. Tests were
129 conducted to determine the heating temperature of the annealing and its effect on the porosity, and
130 the results are displayed in Supplementary Information Figure S1. The relaxation temperature was
131 chosen above 2000K to be in the second part of the curve (the part with the steeper slope) to ensure
132 sufficient relaxation to obtain pores with radii of the order of the experimental ones (around 0.5nm).
133 Overly hot temperatures were also avoided, to prevent the structures from melting with subsequent
134 pore collapse. Finally an intermediate temperature of 2400K was selected. Afterwards the system
135 was instantly cooled to 300 K, at which two successive NVT and NPT (isobaric) relaxations were
136 performed for 20 ps each.

137 Analysis methods

138 King rings

139 Rings were calculated following the King's criterion, which states that a ring is considered the
140 shortest path between a given atom and its nearest neighbours⁴².

141 Pore size distribution (PSD)

142 To estimate the pore morphology and topology of the gels, the pore size distribution can be
143 calculated using the method developed by Bhattacharya and Gubbins⁴³. The pores are explored using
144 a spherical probe of varying size in order to find the largest sphere fitting in the pore. The PSD is
145 defined as the statistical distribution of the radii of these spheres.

146 Coordination number

147 The cut-off radii used to calculate the coordination numbers are given in Table 2. They correspond to
148 the first minimum after the first peak of the radial distribution function.

	Si-O	B-O	Al-O	Na-O	Ca-O
r_{cut} (Å)	2.1	2.0	2.4	3.5	3.2

149 Table 2 – Cut-off radii used for the coordination number analysis

150 Surface atoms

151 To determine the quantity of surface atoms, a method based on the calculation of the local Voronoï
152 volumes was used. For surface atoms located at the pore surface, the local Voronoï volume is larger
153 than for bulk atoms. To identify surface atoms, 3 million points in the simulation box were chosen at
154 random. The number of points nearest to a given atom than any other atoms was calculated for each
155 atom of the system. Hence, the surface atoms can be identified because of a larger quantity of points

156 around them compared to the bulk atoms. A threshold was determined for each gel (Table 3). An
 157 atom is considered to be a surface atom if the number of points around it is superior to this
 158 threshold. Each threshold was determined empirically by verifying visually that it allowed a clear
 159 separation between the surface and the bulk atoms.

	S65.5	S63.0	CJ3	S52.5	S57.5	S51.0
Threshold	75	90	88	86	90	105

Table 3 – Threshold used to identify the surface atoms for each gel

161 Results

162 Structural comparison between simulated pristine glasses and alteration gels

163 Coordination number (CN)

164

		S65.5		S63.0		CJ3		S52.5		S57.5		S51.0	
		Glass	Gel	Glass	Gel	Glass	Gel	Glass	Gel	Glass	Gel	Glass	Gel
Mean CN	Si	4.00	4.00	4.00	3.99	4.00	4.00	4.00	4.00	4.00	4.00	4.00	3.99
	Al	4.01	3.81	4.02	3.67	4.01	3.67	4.01	3.88	4.01	3.70	4.01	3.67
	Ca	6.64	5.67	7.03	4.73	6.97	5.08	6.90	5.87	6.99	5.24	7.04	5.07
NBO (%)	NBO	7.5	3.9	6.8	8.0	5.9	5.8	3.2	5.5	4.5	4.9	3.3	6.0
	O ²	91.4	93.9	92.6	91.8	93.0	93.2	93.7	90.6	93.8	93.1	94.9	92.0
	O ³	1.1	2.2	0.6	0.2	1.1	1.0	3.1	3.9	1.7	2.0	1.8	2.0
Q _n Si (%)	Q ₄	81.2	91.2	82.9	83.6	84.8	87.6	90.8	86.6	87.7	89.0	90.4	86.3
	Q ₃	17.8	8.6	16.3	15.8	14.6	12.0	9.0	12.9	11.9	10.6	9.4	13.2
	Q ₂	1.0	0.2	0.8	0.6	0.6	0.4	0.2	0.5	0.4	0.4	0.2	0.5
	Q ₁	0.0	0.0	0.0	0.0	0.0	0.0	0.0	0.0	0.0	0.0	0.0	0.0
	Q ₀	0.0	0.0	0.0	0.0	0.0	0.0	0.0	0.0	0.0	0.0	0.0	0.0
Q _n Al ⁴ (%)	Q ₄	97.3	97.9	98.0	97.0	98.0	97.5	98.8	97.0	98.7	97.3	99.0	97.2
	Q ₃	2.7	2.0	1.9	3.0	2.0	2.5	1.2	3.0	1.3	2.7	1.0	2.8
	Q ₂	0.0	0.1	0.1	0.0	0.0	0.0	0.0	0.0	0.0	0.0	0.0	0.0
	Q ₁	0.0	0.0	0.0	0.0	0.0	0.0	0.0	0.0	0.0	0.0	0.0	0.0
	Q ₀	0.0	0.0	0.0	0.0	0.0	0.0	0.0	0.0	0.0	0.0	0.0	0.0
Angles (°)	Si-O-Si	151.7	151.4	151.4	150.7	151.4	150.7	152.2	150.5	151.8	150.6	152.4	150.2
	O-Si-O	109.4	109.4	109.4	109.4	109.4	109.4	109.4	109.4	109.4	109.4	109.4	109.4
	O-Al-O	109.2	110.1	109.1	110.9	109.2	110.9	109.2	109.7	109.2	110.6	109.2	110.8
	Si-O-Al	144.1	142.5	143.6	143.6	143.5	143.2	144.3	141.3	143.9	142.0	144.6	141.6
	Al-O-Al	128.8	119.6	129.3	126.3	130.5	121.2	126.7	121.4	126.5	120.9	127.1	122.5
Mean free volume/pore radius (Å)		0.56	1.24	0.54	2.37	0.54	2.01	0.57	3.71	0.56	2.60	0.59	4.46
Mean ring size		5.60	5.25	5.70	5.18	5.66	5.19	5.60	5.11	5.64	5.16	5.78	5.10

Table 4 – Mean CN of Si, Al, and Ca, percentages of NBO, O², and O³, Q_n distribution of Si and Al, calculated mean angle, mean free volume/pore radii and mean ring size in the simulated initial pristine glass and the alteration gels

165 **Table 4** displays the mean CN of Si, Al, and Ca for the glasses and their respective gels. The Si mean
 166 CN remains unchanged between glass and gel, which demonstrates the stability of the silicon
 167 tetrahedron in both glass and gel. However, it can be seen that both Al and Ca mean CN significantly
 168 decrease. For all the glasses, Al is found in tetrahedral form, consistent with experimental data on
 169 aluminoborosilicate glasses^{10,44}. Its mean CN value decreases to between 3.88 and 3.67 in the gels,
 170
 171

172 which shows the presence of 3-fold coordinated Al. This drop is larger when the Al content
173 decreases. A decrease between the Ca mean CN in the gel compared to the glass can also be seen
174 (from a 6.64 – 7.04 range for the glasses to 4.73 - 5.87 for the gels). Non-bridging oxygens (NBO) and
175 the 2 and 3-fold coordinated oxygen percentage are given in the second part of **Table 4**. Globally,
176 they display only minor variations and no clear tendency can be deduced from the NBO %
177 comparison between the glasses and the gels, but the NBO % mostly increase in the gels except for
178 S65.5 and CJ3. Conversely, the O²% decreases in the gels compared to the glasses, with the same
179 exception for S65.5 and CJ3. The O³% is less than 3%, except for S52.5. While the existence of these
180 species has never been confirmed experimentally, several molecular dynamics studies have shown
181 their existence in equilibrated glasses⁴⁵⁻⁴⁷. In our compositions, the O³% increases with the Al %
182 content **in the gels and a similar trend is observed for the glasses (except for S65.5 and S57.5)**, which
183 could indicate that the O³ entities play a role of charge compensator. The O³% increases in the gel
184 compared to the glass, except for S63.0 and CJ3.

185 Additionally, Si and Al⁴Q_n species were calculated for glasses and gels alike (**Table 4**). It appears that
186 the Si Q₄ percentage generally increases at the expense of Q₃ in the gels compared to their glasses,
187 except for S52.5 and S51.0 for which the percentage decreases. These two glasses have the lowest
188 SiO₂ percentages. S65.5 shows the greatest increase in Q₄, from 81.2% to 91.1%, which can be
189 attributed to the low soluble/insoluble ratio and the higher Si percentage. Furthermore, the Si Q₄
190 percentage is higher than that observed experimentally¹⁰. It could be related to a faster
191 reconstruction of the Si at the expense of the Al. Changes in the Q_n population relative to Al⁴ appear
192 to be negligible.

193 **Angle**

194 The mean angle values of different M-O-M or O-M-O (M = Si, Al) linkages in both glasses and gels can
195 be found in **Table 4**. It appears that for all the gels, the Si-O-Si, Si-O-Al (except S63.0), and Al-O-Al
196 angle values decrease, with a larger decrease for the latter. While the O-Si-O mean value remains
197 constant, ranging from 109.36 to 109.60° (standard value for the tetrahedron angle), the O-Al-O
198 angle slightly increases in the gels compared to the glasses. This can be explained by an increase in
199 the Al³ quantity, creating trihedra with internal angles close to 120°.

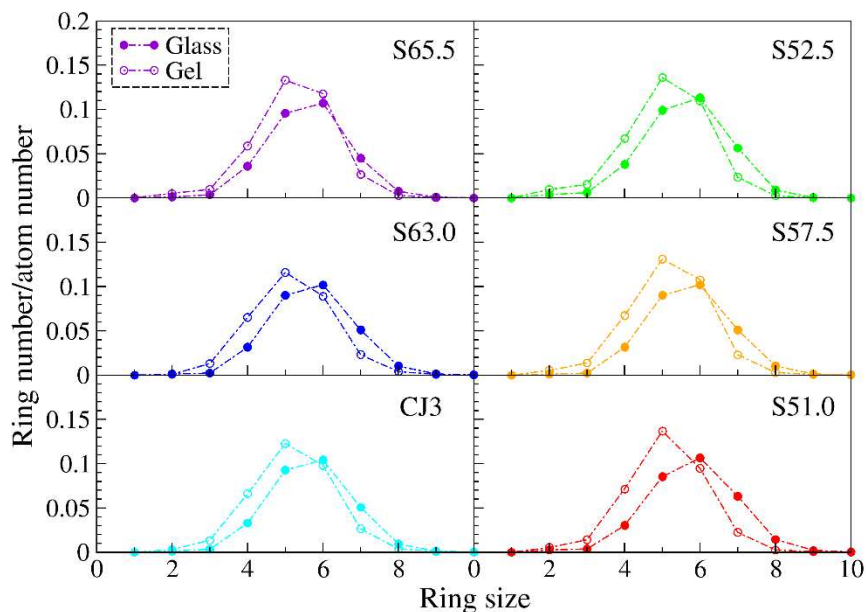
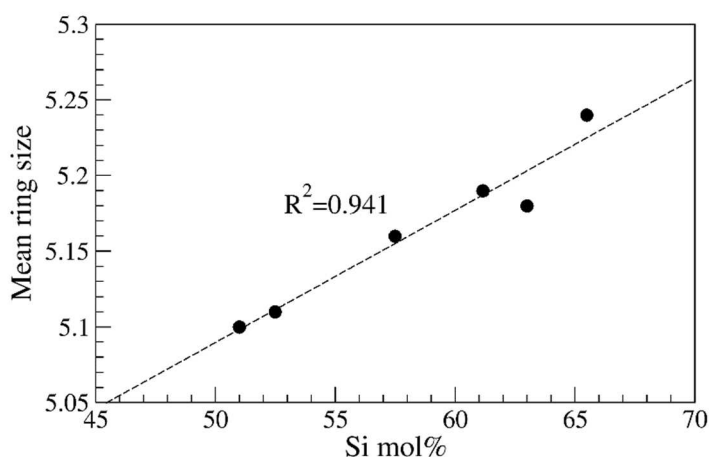
201
202

Figure 1 – Distributions of King ring sizes in the initial glasses and in the dry gels

203 Figure 1 shows the King ring size distribution⁴² for both glasses and gels. It appears that in the glasses
 204 the maximum ring population is centred at a value of 6, while it is centred on 5 in the gels. The ratios
 205 of mean ring size between a gel and its parent glass were calculated. From these results, it can be
 206 seen that the glasses with the same soluble/insoluble ratio had roughly the same values, ranging
 207 from 0.910 to 0.918. However, the S65.5 (lowest S/I ratio) had the highest ratio with a value of 0.938,
 208 while the S51.0 (highest S/I ratio) had the lowest value, at 0.883. Additionally, it can be noted from
 209 Figure 2 that the mean ring value in gels decreases almost linearly ($R^2=0.941$) with the Si %, which is
 210 equivalent to the (B+Al) content.



211

212

Figure 2 – Evolution of the mean ring size of the gel with Si content (mol%) in the initial glass

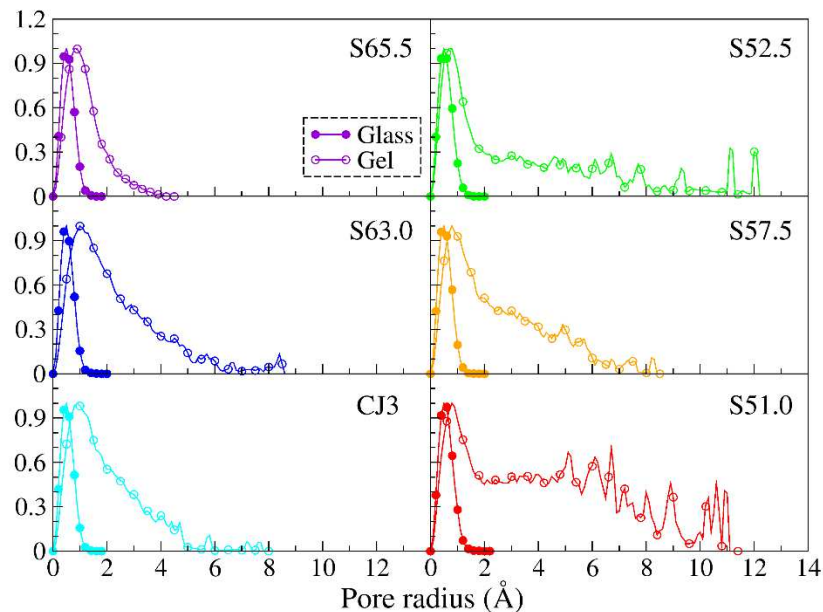
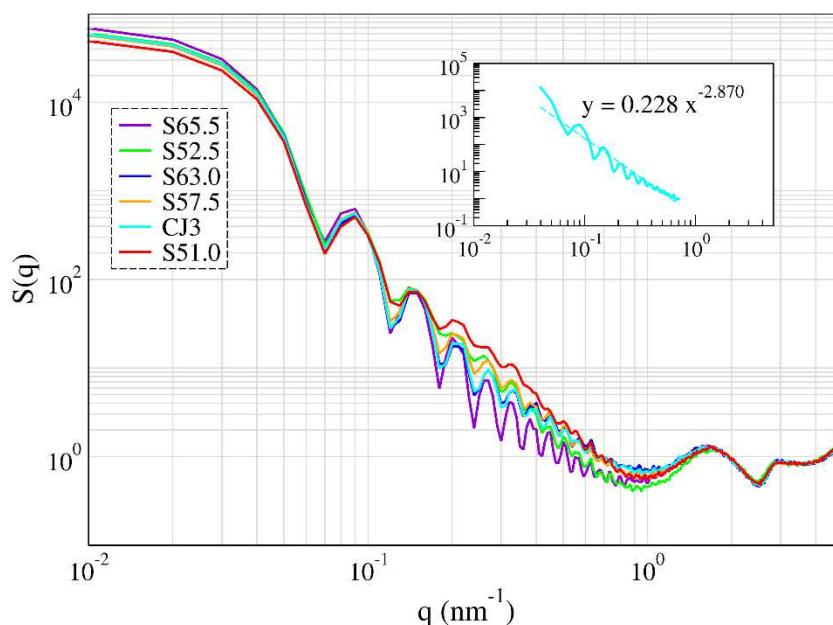
214
215

Figure 3 – Pore size distribution in the initial glasses and in the dry gels

216 The pore size distribution (PSD) was calculated for the dry gels and the initial glasses as a reference
 217 for the free volume intrinsic to the glasses, using the method of Bhattachary and Gubbins⁴³.
 218 Hereafter are considered as 'pores' only the volume that enables the transport of an H₂O molecule,
 219 thus pores with a radius larger 1.25 Å, which correspond to the maximum free volume visible in the
 220 glasses. These results are presented in Figure 3. It can be seen that for all the glasses, the PSD is
 221 roughly the same, with a maximum of distribution at around 0.5 Å which slightly increases with a
 222 decrease in density. However, the shapes of the PSD differ significantly between the gels. The pore
 223 radius is at its maximum for the gels prepared from the glasses with the highest B content, and then
 224 decreases as the B content in the glasses decreases.



226
227

Figure 4 –Structural factors $S(q)$ of the simulated alteration gels

228
229

	S65.5	S63.0	CJ3	S52.5	S57.5	S51.0
n	3.165	2.824	2.870	3.169	2.906	2.853

230

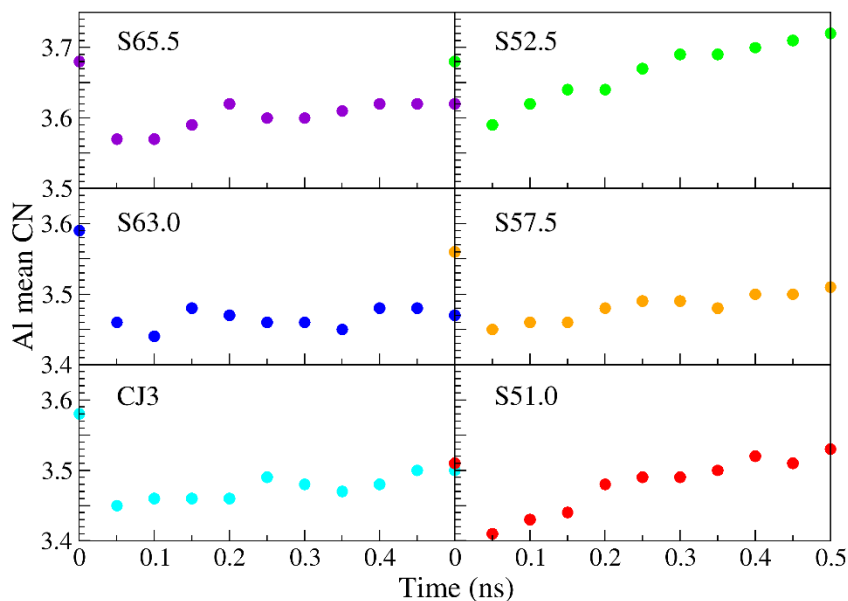
Table 5 – Exponent n extracted from a fit of the structure factors by the power law q^{-n} in the dry gels

231 The structure factors $S(q)$ derived from the calculated SAXS spectra were obtained following the
 232 same method as that used by Cailleateau et al.¹⁴. The results are presented in Figure 4. While the
 233 shape of the curve fluctuates considerably (certainly induced by the relatively small size of the
 234 system), the exponent n can be calculated from the power law q^{-n} regression in order to evaluate the
 235 regularity of the pores. Between 1 and 3 the exponent is indicative of the pore structure, whereas
 236 between 3 and 4 it is representative of the surface of the pores. In fact, an increase in the pore
 237 regularity corresponds to an increase in the exponent from 3 to 4. The exponent values for the dry
 238 gels can be found in Table 5. As they remain relatively close (2.82 to 3.17) despite the wide
 239 composition range, it seems to have little effect on the pore regularity.

240

241 Structural evolution of the “dry” gels during the annealing at 2400 K

242 Coordination number



243
244

Figure 5 – Aluminium CN in the dry gels versus time during the annealing at 2400 K

245 Figure 5 and Figure 6 display the time dependency of the mean Al CN and Ca CN, respectively, during
246 the 0.5 ns annealing stage at 2400 K. For all the gels, a major decrease can be observed immediately
247 after the beginning of the annealing relaxation due to the thermal motions (the temperature was
248 raised from 300K to 2400K for the annealing). The coordination numbers in the gel structures
249 equilibrated at 300K are given in Table 4, but this section shows how the dynamics of dry gel
250 formation occur during the annealing stage at 2400K.

251 Hereafter, a reconstruction of the Al⁴ and Ca environments occurs, with its efficiency depending on
252 the gel. From these results, two behaviours can be deduced: gels for which the reorganisation is only
253 slight (S65.5, S63.0, CJ3), and gels for which the reorganisation is more developed (S52.5, S57.5,
254 S51.0).

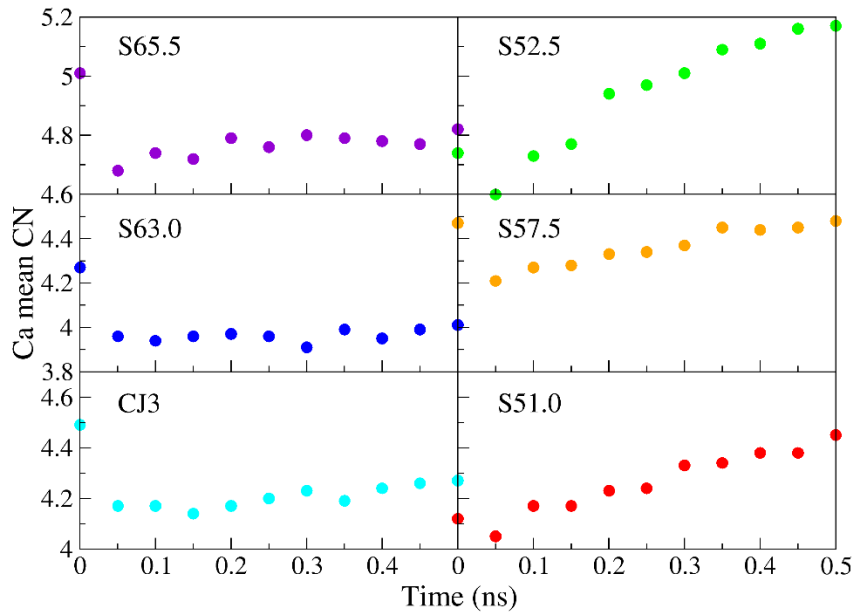


Figure 6 – Calcium CN in the dry gels versus time during the annealing at 2400 K

255
256

257 **NBO and O³**
258

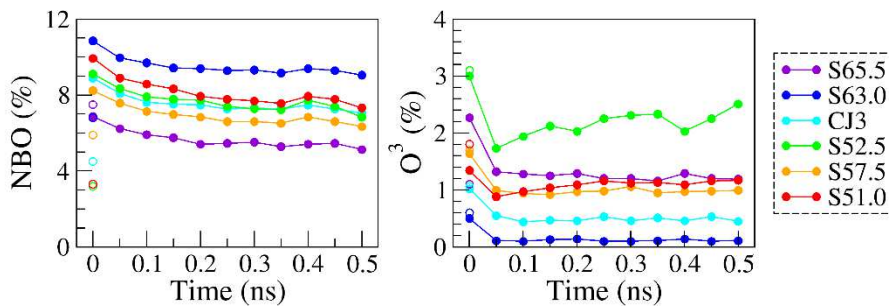
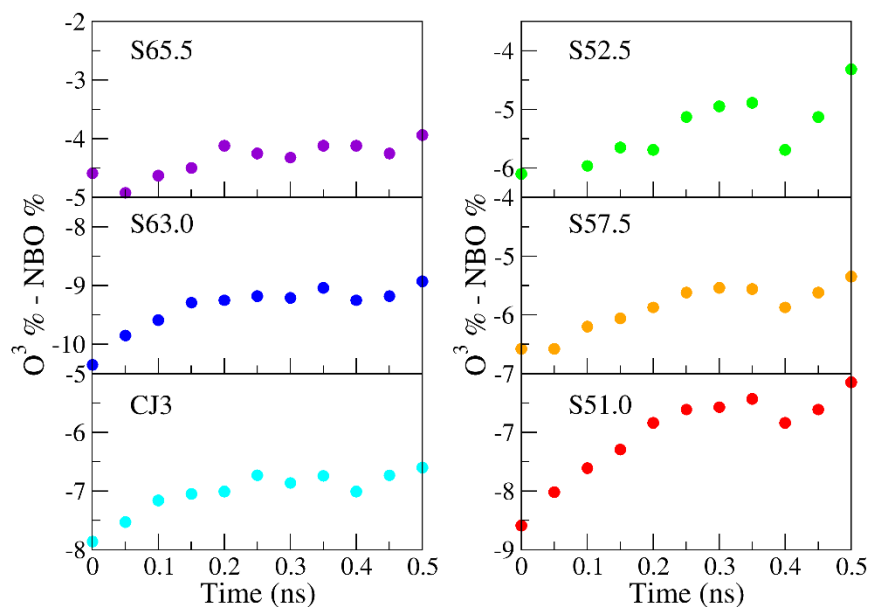


Figure 7 – NBO and O³ percentages evolution of the dry gels versus time during the annealing at 2400 K. Empty symbols represent the NBO and O³ percentages in the initial glasses.

259
260
261

262 Figure 7 displays the evolution of the NBO and O³ percentages through the annealing at 2400K. One
 263 can see through the comparison between the NBO percentage in the initial glass and at the
 264 beginning of the annealing, that the removal of the B and Na induces a significant increase of NBO
 265 percentage (except for S65.5, which shows a slight decrease). The NBO percentage then decreases by
 266 roughly 2 % during the annealing and is stabilised quite quickly after around 0.2 ns. The comparison
 267 between the O³ percentage in the initial glass and at the beginning of the annealing displays few
 268 modifications (except for S65.5, which shows an increase and S51.0, which shows a decrease). During
 269 the annealing at 2400K, the O³ percentage is stabilised rapidly at 0.05 ns. It can be noted that the O³
 270 % increases with the Al % in the glass, confirming what has been shown previously in the glass and in
 271 the final gel (see Table 4).

272 During annealing at 2400K, the NBO percentage decreases and the O³ percentage increases. It means
 273 that there is a global increase of the polymerization level of the structures. A correlation between the
 274 Al coordination change (Figure 5) and the polymerization level change can be noted. The
 275 polymerization level change has been estimated by calculating the quantity %O³ - %NBO (Figure 8).
 276 Globally, the larger the increase of the polymerisation level, the larger the increase of the Al
 277 coordination during annealing.



278

279

Figure 8 – Evolution of O3% - NBO% of the dry gels versus time during the annealing at 2400 K

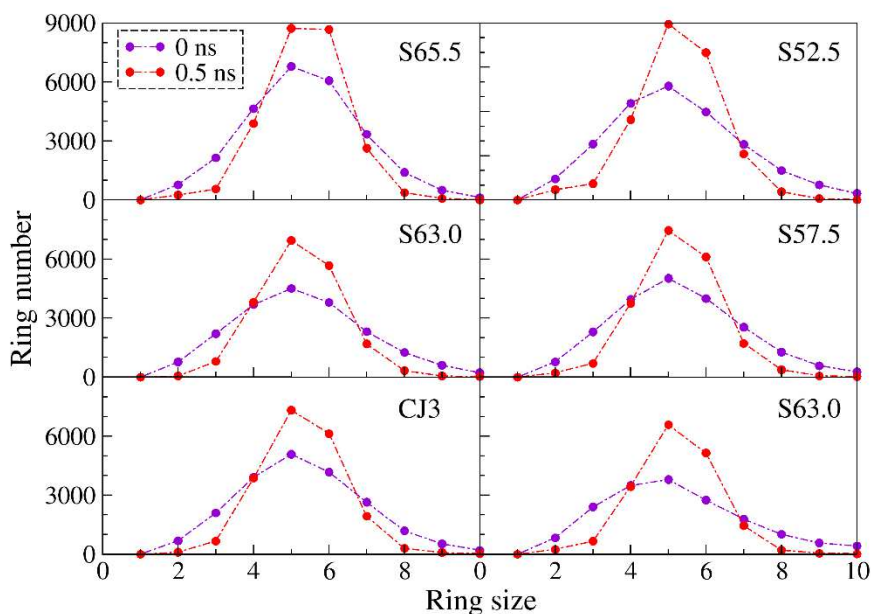
281
282

Figure 9 – King ring size distributions in the dry gels before and after the annealing at 2400 K

283 The King ring size distribution just before and immediately after the annealing are compared in
 284 Figure 9. The presence of 2-membered rings at the beginning of the annealing but no longer visible at
 285 the end is coherent with the observation of few Si-O-Si, O-Si-O, and Si-O-Al angles equal to 90° (not
 286 shown here). All distributions are centred on 5-membered rings. A narrowing of the distribution is
 287 observed for the six gels after annealing. A characteristic “reorganisation” time τ , corresponding to
 288 the reconstruction of the network at 2400 K, can be estimated by fitting the FWHM (Full Width Half
 289 Maximum) change with time during the annealing as $FWHM = A + Be^{-t/\tau}$. From these values,
 290 displayed in Table 6, it seems that a lower Si content is associated with a longer relaxation time,
 291 which can probably be ascribed to a more flexible network (the S65.5 structure is an exception).
 292 However, this correlation remains weak.

	S65.5	S63.0	CJ3	S52.5	S57.5	S51.0
τ (ns)	0.0620	0.0479	0.0467	0.0592	0.0606	0.0560

293 Table 6 – Characteristic “reorganisation” time τ estimated from the narrowing versus time of the King ring size distribution
 294 of the gels during the annealing at 2400 K

295

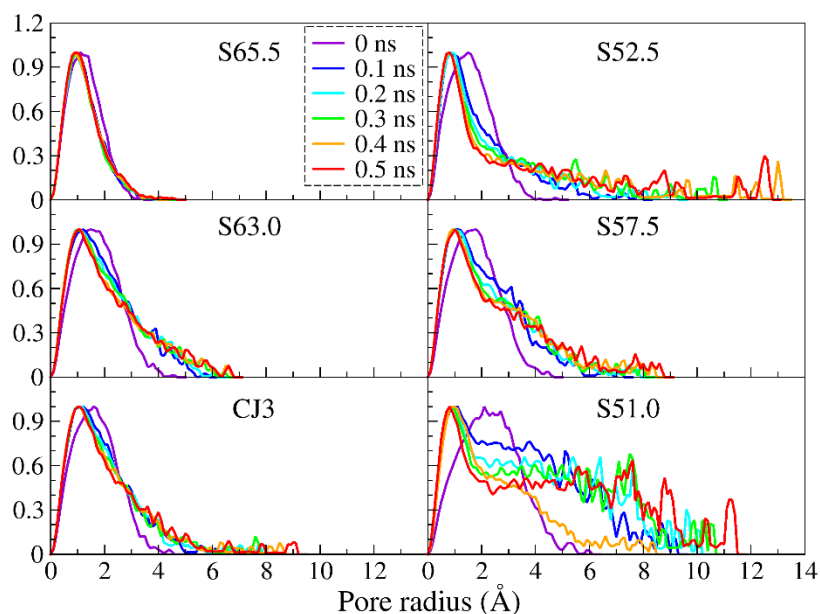
297
298

Figure 10 – PSD evolution of the dry gels versus time during the annealing at 2400 K

299 From the PSD evolution versus time illustrated in Figure 10, the formation of pores with greater radii
 300 can be observed for all the gels, but the increase in progressive distribution spreading strongly
 301 depends on the composition. For S57.5, S52.5, and S51.0, a larger and faster spreading of the
 302 distributions can be observed compared to CJ3, S63.0, and S65.5. The ratio of the final compared to
 303 the initial mean pore radius has been calculated from values displayed in Supplementary Information
 304 Figure S2 and evolves as S52.5 > S51.0 > S57.5 > CJ3 > S63.0 > S65.5. This confirms the two
 305 behaviours previously identified. The gels formed from glasses with a lower Si content (S52.5, S51.0,
 306 S57.5) present a more developed reorganisation than the gels formed from glasses with a higher Si
 307 content (S65.5, S63.0, CJ3).

308 Surface atoms

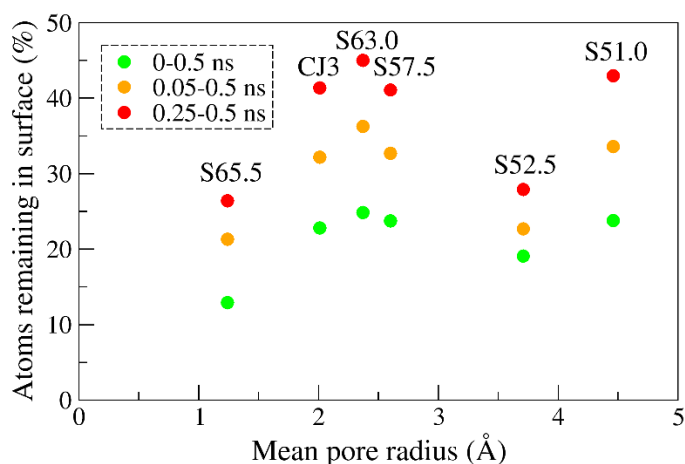
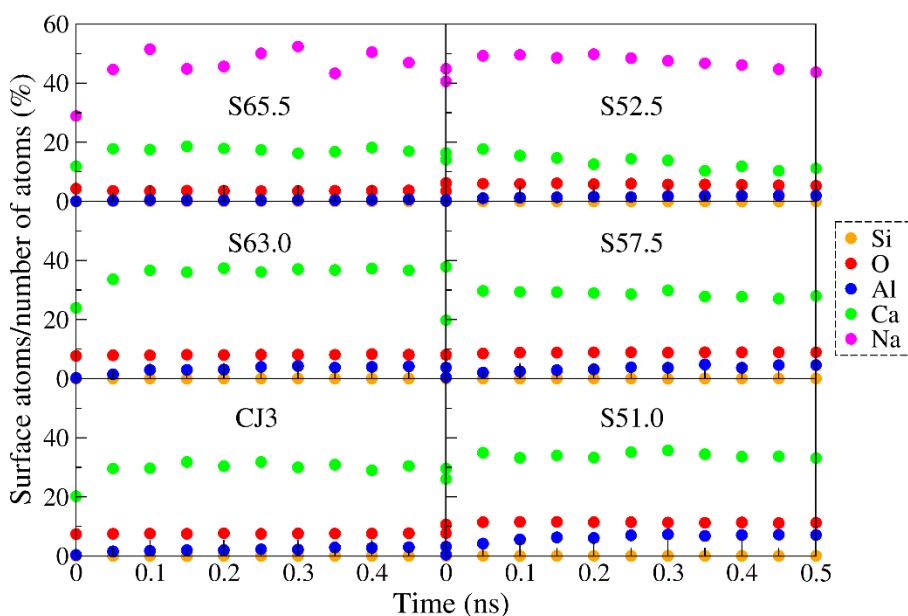
309
310
311

Figure 11 – Evolution of the percentage of atoms remaining at the pore surfaces during different time intervals of the annealing versus the mean pore radius of the gels

312 The number of atoms on the pore surfaces was calculated for all the gels. Their evolution through
 313 time can be found in the Supplementary Information Figure S3. It appears that the number of surface
 314 atoms mainly increased at the beginning of the annealing for most of the gels, then remained fairly
 315 constant (or decreased slightly for S52.5). Also, the number of surface atoms is directly linked to the
 316 number of atoms removed initially, as shown in Supplementary Information Figure S4.

317 However, even if the number of surface atoms remained roughly constant, it appears (Figure 11) that
 318 only $\approx 20\%$ of the atoms initially present on the surface at the beginning of the annealing were still on
 319 the pore surfaces at its end. This is indicative of a fast reorganisation during the annealing. It is
 320 nevertheless greater at the beginning of the relaxation, as between 0.05 and 0.5 ns at least 30% of
 321 the atoms remained on the pore surfaces for most of gels. Additionally, during the second half of the
 322 relaxation nearly 40% of the surface atoms were stabilised on the pore surfaces, which is indicative
 323 of a slowing down of the gel reorganisation. No clear trend between the number of surface atoms
 324 and the pore size is recognisable.

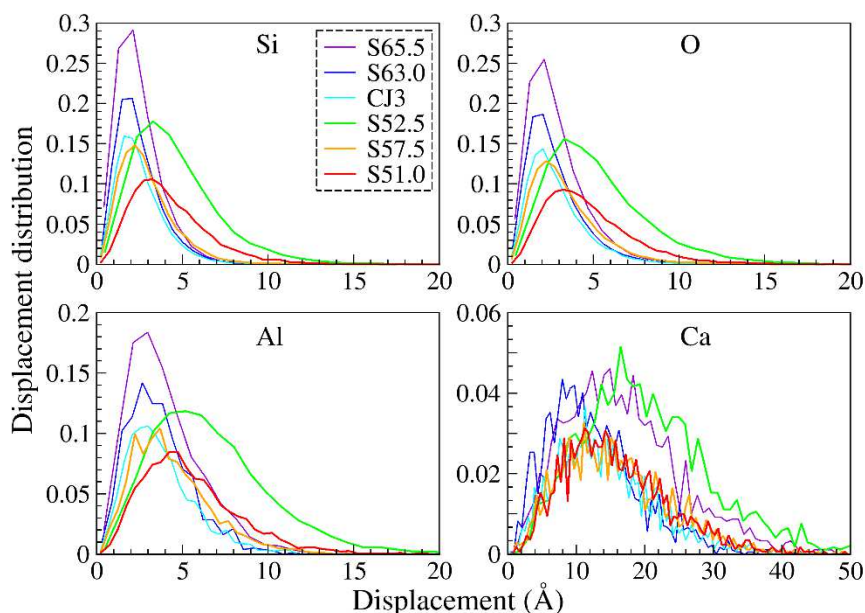


325
 326 *Figure 12 - Evolution of the percentage of atoms on the pore surfaces (relatively to the total number of atoms in the system)*
 327 *versus time for the different atom species*

328 The surface atom types were investigated (see Supplementary Information Figure S5). It appears that
 329 some atom types are more likely to be at the pore surfaces. For all gels, the O atoms were
 330 predominant and they represented roughly 80% of all the pore surface atoms. Then followed Na (for
 331 S52.5), Ca with $\approx 15\%$, Al within the 1-4% range, and finally Si with less than 0.2%. Furthermore, when
 332 normalised to the total quantity of atoms of a given type, it seems from Figure 12 that mobile
 333 elements such as Na and Ca can be found in a higher proportion at the pore surface compared to O,
 334 Al, and Si. It should be noted that at least 50% of Na atoms were present on the pore surfaces for the
 335 two Na-containing gels. For these, 20% of the calcium atoms were surface atoms whereas on the Na-
 336 depleted gels, their proportion increased to reach values between 30 to 40%. It is interesting to see
 337 that Na-containing gels carry just enough Na to compensate all the Al. However, if 50% of them are

338 on the pore surfaces, they are no longer available for charge-compensation. This could partially
 339 explain the high number of 3-fold coordinated Al in the gels.

340 Atomic displacements



341
 342 *Figure 13 – Displacement distributions of Si, O, Al, and Ca during the dry gel annealing at 2400 K.*

343 **Figure 13** shows the atomic displacement distribution of the six gels for Si, O, Al, and Ca. The mean
 344 values of these distributions are presented in Supplementary Information Figure S6. From these
 345 Figures it can be seen that the mobility of the different types of atoms increased as $Si < O < Al < Ca$.
 346 The higher mobility of aluminium compared to oxygen is unexpected, as the opposite is generally
 347 documented when diffusion is calculated at different temperatures in equilibrated glasses.
 348 Moreover, the mobility of the atoms depends on the gel composition. The atomic displacements in
 349 the S52.5, S51.0, and S57.5 gels were greater than in the S63.0, S52.5, and S65.5 gels (except for the
 350 Ca in S65.5). The atomic displacements represent further evidence that the gels formed from glasses
 351 with a lower Si content **reorganise** more during the annealing at 2400K.

352

	τ_{Si} (ns)	τ_O (ns)	τ_{Al} (ns)	τ_{Ca} (ns)
S65.5	0.065	0.068	0.081	0.162
S63.0	0.059	0.060	0.067	0.117
CJ3	0.062	0.065	0.069	0.132
S52.5	0.135	0.129	0.133	0.149
S57.5	0.073	0.075	0.087	0.134
S51.0	0.087	0.086	0.094	0.137

353
 354 *Table 7 – “Reorganisation time” τ calculated from the average displacement versus time for Si, O, Al, and Ca in the simulated gels during the annealing relaxation at 2400 K*

355 In **Table 7** can be found the characteristic “reorganisation” time τ associated with the Si, O, Al, and Ca
 356 displacements. These values were calculated by fitting the average displacements per atom type

357 versus time with $\bar{S}(t) = A(1 - e^{-t/\tau})$. For each gel, comparison of τ per atom type reflects the same
358 trend as previously seen, following Si < O < Al < Ca. The higher the “reorganisation” time of an atom
359 type, the longer it moves. The Ca showed the greatest mobility, probably due to its network modifier
360 role, and was therefore less impacted by the polymerised network. Also, when comparing the
361 different gels, it can be seen that the characteristic “reorganisation” time for all the atom types
362 evolved as S52.5 > S51.0 > S57.5 > S65.5 > CJ3 > S63.0 (except for the Ca in S65.5, which was higher
363 than all the other gels), confirming the two possible behaviours of a gel depending on the Si content
364 in the initial glass.

365 Discussion

366 Structural changes between the initial glass and the dry gel

367 Local order

368 Some local order structural differences can be pointed out between the glasses and their gels. The
369 removal of all boron atoms seemed to trigger the formation of a more polymerised silicon network
370 for the majority of the gels, with the increase of Si Q₄ species at the expense of Q₃. While this trend
371 has been suggested by NMR experimental results obtained by Collin et al. on the ISG¹⁰, it was also
372 noted that the decrease of the chemical shift for Si could be the result of a second-neighbour effect
373 and not come from a higher polymerisation degree. In the case described here, the overall increase
374 in Q₄ species could be the result of a surface effect, as a large proportion of the network modifiers
375 were present on the surface of the pores and thus not available to form NBOs. This effect may
376 disappear in further simulation when water is added, creating silanol groups at the pore surface.
377 However, the opposite phenomenon was observed for the S51.0 and S52.5 gels, for which a decrease
378 of Si Q₄ species of around 4% was observed. These gels were prepared from the glasses with the
379 lowest silicon content, respectively 51% and 52.5% (and also the highest boron content). This
380 decrease may originate from the high number of charges to be compensated in the original glasses,
381 thus limiting the number of NBOs, which then increases in the gels. Conversely, the largest change in
382 the Q_n population occurred for the S65.5, which was the glass with the highest (63%) silicon content.
383 Between the S65.5 glass and its gel, Si Q₄ species increased by 10%. Therefore, the least destabilised
384 glasses seem to lead to a more reticulated gel network. It can also be noted that NBOs were more
385 often found attached to silicon atoms rather than aluminium atoms. Allwardt et al.⁴⁸ had already
386 observed this experimentally. As stated earlier, an increase in the number of tricoordinate oxygens
387 can be observed in the gels compared to the glasses. This suggests that the stabilisation of some
388 four-fold coordinated aluminium in the gels is achieved by O³ entities⁴⁹, even if the theoretical total
389 number of charges would enable a full compensation of aluminium atoms.

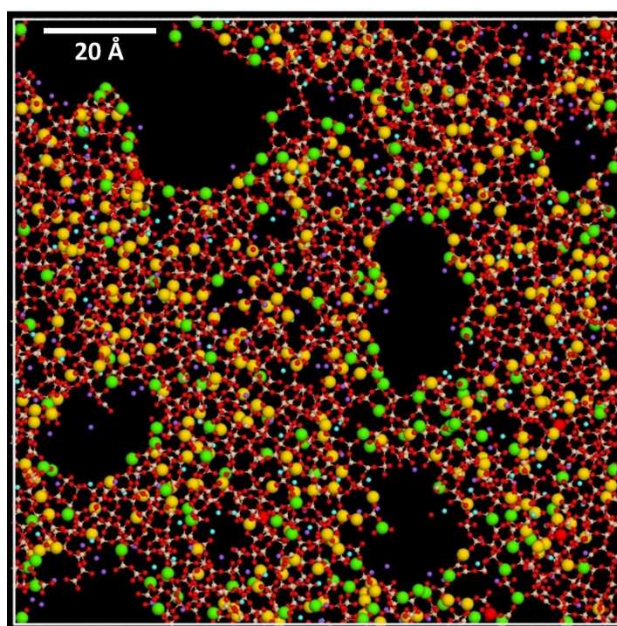
390 Effect of the initial perturbation induced by the removal of B and Na

391

392 The most apparent effect of the initial perturbation, namely the removal of B and Na, can be
393 observed on the pore size of the gels. The mean pore size as well as the global pore size distribution
394 increased with an increasing boron content in the initial glass, as seen in Figure 3. Across the
395 compositional range studied, the mean pore radius values range from 1.25 Å up to 4.5 Å.
396 Additionally, the variations in composition lead to different maximal pore radii, up to 12 Å for S52.5.
397 Considering the wide range of pore sizes obtained from the various compositions, it seems
398 appropriate to evaluate the impact of both the size and surfaces of the pores on the structure of the
399 surrounding gel network.

400 Several variations in coordination as well as in bond angles are attributed to surface effects, meaning
401 their relatively higher occurrence at the surface of pores. The increase of three-fold coordinated
402 aluminium as well as the decrease in calcium coordination number can be indicative of such effects.
403 As can be seen in **Figure 14**, the 3-fold coordinated Al appears to be mostly present at the surface of
404 the pores compared to the 4-fold coordinated Al. Moreover, the study of the surface atoms indicates
405 that, on average, 97% of the Al on the pore surfaces are 3-fold coordinated. The decrease in the
406 coordination number could also be ascribed to the global depletion in oxygen atoms, necessary to
407 maintain charge neutrality in the gels (see Methods), which is intrinsically linked to the pore surface.
408 Furthermore, a large proportion of the charge compensators were found on the pore surface, thus
409 not available for charge compensation in the gel network. It can also be noted that the increase in
410 three-fold coordinated aluminium seems to be larger when the aluminium content decreases
411 through the series. However, this could be the result of statistical effects as no clear correlation can
412 be determined.

413 As a result, a slight increase (up to nearly two degrees) in the mean O-Al-O angle was observed,
414 which is consistent with an increasing population of Al³ tending to reach a 120° trihedral angle.
415 Additionally, Si-O-Si and Si-O-Al mean angle values decreased in the gels compared to the glasses,
416 which is consistent with observations reported elsewhere^{35,36} and attributed to surface effects.
417 However, when compared to Rimsza et al.³⁶, the decrease appears to be much smaller: around 1-2°
418 here, compared to approximately 9° in their work. In order to better understand the origin of this
419 effect, it is necessary to study the dynamics of gel formation.



420
421 **Figure 14** – View of a slice of the S52.5 gel. Large atoms are 3-fold coordinated Al atoms in green, 4-fold coordinated in
422 yellow, and 5 fold-coordinated in red. Small spheres represent: in beige, Si atoms; in red, oxygen atoms; in purple, Na atoms;
423 and in cyan, calcium atoms.

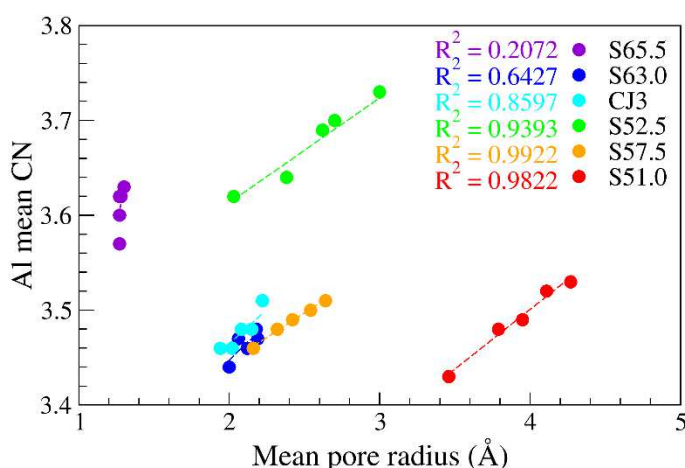
424 The dynamics of the gel **reorganisation** points to two distinct behaviours that seem to originate from
425 the initial degree of **destabilisation** undergone by the materials after the removal of B and Na. The
426 displacement distributions for the different species give the first insights into the **reorganisation**
427 within the gels. It can be seen that while calcium atoms were the most mobile cations during the
428 **reorganisation**, aluminium atoms came just after them. This may be because highly distorted
429 aluminium sites lead to a greater relaxation. In equilibrated glasses, it has been generally observed
430 that the Al atoms displace less than the O atoms. The contrary was observed here, probably because

431 of the large initial perturbation associated with the B and Na removals. As a consequence, Al atoms
432 needed to displace more to rebuild their **stable** environments.

433 Additionally, two behaviours were clearly seen among the gels, with S65.5, S63.0, and CJ3 showing
434 the lowest displacements for all atom types, as opposed to S52.5, S51.0, and S57.5, which showed
435 the highest mobility and thus a greater **reorganisation**. Several other features at different range
436 orders support this result. On the intermediate range order, it appears from the PSD (**Figure 10**) and
437 the mean pore size (Supplementary Information) that the evolution of the pore sizes within the gels
438 depends on the gel composition. Pore size exhibits a larger increase for the gels (S52.5, S51.0, S57.5)
439 formed from the glasses with lower Si % content, and alternatively greater (B+Al) % content. The
440 highly disrupted shape of the PSD for these gels suggests that there might be more interconnected
441 pores than in the gels formed from glasses presenting a larger Si % content³².

442 On the short-range order, the evolution of the mean CN for both Al and Ca during the **reorganisation**
443 process validated the existence of two categories of gels with distinct relaxation degrees. Again,
444 S52.5, S51.0, and S57.5 showed a greater increase of these CN and thus a better reconstruction of
445 the local environments around these atoms compared to the S65.5, S63.0, and CJ3 gels.
446 Furthermore, when comparing the evolution of the Al and Ca mean CN with the mean pore radius
447 during the **reorganisation** of the different gels, the two distinct behaviours appear even more clearly.
448 **Figures 15 and 16** display the Al CN and Ca CN, respectively, as a function of the mean pore radius
449 during the annealing at 2400K. In the three gels S52.5, S57.5, and S51.0, a linear evolution of the Al
450 and Ca CN with the mean pore size can be observed. This result is a supplementary indication that
451 two types of behaviours can be identified, with S52.5, S57.5, and S51.0 corresponding to the gels that
452 present the largest and longest reorganisation, as opposed to S65.5, S63.0, and CJ3 which show only
453 slight signs of **reorganisation**. This can be linked to the initial **destabilisation** of the gels. Furthermore,
454 for the S52.5, S57.5, and S51.0 gels, the slopes in **Figures 15 and 16** are the same for Al on one part
455 and Ca on the other part (3 times higher for Ca than for Al). This could indicate that one elementary
456 change in one Al or one Ca local environment is associated with the same variation of the pore
457 volume, irrespective of the gel composition.

458



459

460 **Figure 15** – Aluminium CN evolution versus the mean pore size in the dry gels during the annealing at 2400 K

461

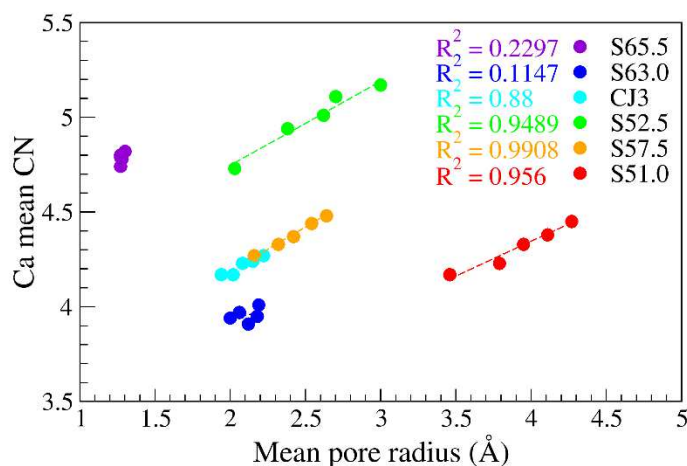


Figure 16 – Calcium CN evolution versus the mean pore size in the dry gels during the annealing at 2400 K

462
463

464

465 Comparison with literature

466

467 The results we obtained can be considered to be at an interface between earlier work performed by
468 Rimsza and Du on “dry” silica gels³⁶, and work on gels formed from multicomponent glasses³² using
469 different methods.

470 The first comparison is made with a recent work performed on hydrated gel structures³² using the
471 REAXFF method. The gels were obtained with two different methods: introduction of a hydrogarnet
472 defect on dense silica and removal of three different percentages of Si atoms, and soluble species
473 removal from a simplified international simple glass (sISG). In the study presented here, water was
474 not present. Comparison between dry and hydrated materials should provide insights into the
475 mechanisms by which gels form and evolve. Furthermore, the gels studied here contained Si, Al, Ca,
476 and some contained Na, while in Rimsza and Du’s work, the gels were formed from pure silica. Also,
477 our systems are two orders of magnitude larger. Similar results were nevertheless obtained for the
478 ring size distributions, with values centred on five-membered rings. It should be noted that for our
479 glasses, the ring size centred around six-membered rings, which differs from what was obtained for
480 the sISG (centred around five) and which is comparable to CJ3 (with 5.81% of Ca substituted for
481 Na₂O). Another difference resides in the number of Si Q_n species, as we found between 81% and 91%
482 Q₄ in both glasses and gels with the rest being mainly Q₃, while there was only a rather small
483 percentage of Q₄ in their system (around 10%). However, both methods present some degrees of
484 repolymerisation between the simulated glass and the gel, with an increase in Q₄ at the expense of
485 Q₃ in our case, and an increase of Q₃ and Q₄ at the expense of Q₂ and Q₁ in their case. This difference
486 could be explained by the fact that there was no water in our systems, or because the Q₄ percentage
487 was initially higher in our CJ3 glass. Finally, the PSD we obtained do not have the same or similar
488 shapes as those they obtained. This might primarily be due to a larger system which enabled bigger
489 pores to form in our study samples. However the S65.5 gel, despite its larger size, was the only one
490 that displayed a similar shape. Nevertheless considering the differences in compositions, no clear
491 correlation can be found.

492 It is also interesting to compare the work described here with Rimsza and Du’s work on dry gels³⁶.
493 The dry gels they studied were silica gels obtained using two different methods called volume scaling
494 (VS), for which the cell volume size is linearly increased from dense amorphous silica, and charge

495 scaling (CS), which consists in simulating nanoporous silica by increasing the ionic charge for each
496 simulation step. For both methods they observed an increase in structural defects, mainly the
497 presence of three-fold coordinated Si with increasing porosity. It is interesting to note that in the
498 absence of other elements, defects appeared on Si (up to 6% Si³ with the VS method), while in our
499 study the Si remained tetra coordinated and the defects concentrated around the Al local
500 environments. This confirms the high stability of the SiO₄ tetrahedron compared to the AlO₄
501 tetrahedron. When comparing the angle distributions, in Rimsza and Du's study the formation of a
502 small shoulder at 90° can be seen, indicative of the presence of two-membered rings, mainly near
503 the surface of the pores. This was also clearly visible in our gels. However, the shoulder disappeared
504 after relaxation because the two-membered rings are easily annealed. It can also be observed that
505 the **maximum of the Si-O-Si bond angle distribution decreases** when using the VS method, due to
506 both a variation in density as well as surface effects. This was however not observed with the CS
507 method. It thus appears that our method is closer to the VS method, which is more representative of
508 a chemical vapour deposition (CVD) process in terms of pore morphology, than to the CS (more like
509 sol-gel processing).

510 Conclusion

511

512 To sum up, this study focussed on dry gels obtained from alumino-borosilicate glasses with varying
513 soluble/insoluble and SiO₂/Al₂O₃ ratios in order to investigate the impact of glass compositions on gel
514 properties. A new method is proposed, consisting in removing the B and Na atoms from the glass and
515 annealing the resulting structure at high temperature.

516 We analysed primarily the pore size and morphology. As expected, the mean pore radius increased
517 with increasing boron content in the glass, but interestingly various maximal pore sizes were found
518 which could be indicative of interconnected pores. Most of the structural defects were found on Al,
519 and lead to an increase in three-fold coordinated aluminium, especially at the pore surfaces. This
520 surface effect was confirmed by a decrease in the Si-O-Si and Si-O-Al **mean** angles.

521 The study of the **reorganisation** dynamics of the different gels highlighted two distinct behaviours
522 which did not correspond to the hypotheses emitted when designing the compositions. The gels
523 formed from the glasses with the largest Si content displayed the lowest displacements for all the
524 atomic species, as well as the smallest pore sizes and recovery of the Al and Ca local environments,
525 as opposed to the gels formed from the glasses with lower Si content. This is indicative of a larger
526 and longer **reorganisation** of the gels when the initial perturbation is higher. Interestingly, it was
527 shown that while Ca is the most mobile cation, it was closely followed by Al, which was not expected
528 as Al mobility is usually less than that of O in equilibrated glasses. It is thus suggested that both their
529 displacements are interdependent to some extent, and considerable **reorganisations** occur around
530 the Al and Ca atoms during the gel **reorganisation**. This has also been pointed out by the linear
531 evolution of both Al and Ca mean CN with the mean pore radius for the gels that reorganize the
532 most.

533 Finally, the comparison with works performed by Rimsza and Du^{32,36} enabled us to find qualitatively
534 similar results, with the decreased ring size in certain gels compared to glasses, as well as defects
535 concentrated at the pore surfaces. The next step is to add water to our systems, in order to fully
536 characterize more realistic gels. This may well have effects on the gel structures and pore surfaces.

537

538 Acknowledgement

539
540 This work was supported as part of the Center for Performance and Design of Nuclear Waste Forms
541 and Containers, an Energy Frontier Research Center funded by the U.S. Department of Energy, Office
542 of Science, Basic Energy Sciences under Award # DE-SC0016584. The authors are grateful to Jincheng
543 Du and his team (University North Texas) for the work done on the potentials development.

544 References

- 545 1 Morse, D. L. & Evenson, J. W. Welcome to the Glass Age. *Int J Appl Glass Sci* **7**, 409-412,
546 doi:10.1111/ijag.12242 (2016).
- 547 2 Gin, S. *et al.* An international initiative on long-term behavior of high-level nuclear waste
548 glass. *Mater Today* **16**, 243-248, doi:10.1016/j.mattod.2013.06.008 (2013).
- 549 3 Vienna, J. D., Ryan, J. V., Gin, S. & Inagaki, Y. Current Understanding and Remaining
550 Challenges in Modeling Long-Term Degradation of Borosilicate Nuclear Waste Glasses. *Int J*
551 *Appl Glass Sci* **4**, 283-294, doi:10.1111/ijag.12050 (2013).
- 552 4 Donald, I. W. *Waste immobilization in glass and ceramic based hosts: radioactive, toxic and*
553 *hazardous wastes.* (John Wiley & Sons, 2010).
- 554 5 Grambow, B. Nuclear waste glasses - How durable? *Elements* **2**, 357-364, doi:DOI
555 10.2113/gselements.2.6.357 (2006).
- 556 6 Gin, S. *et al.* Nuclear Glass Durability: New Insight into Alteration Layer Properties. *J Phys*
557 *Chem C* **115**, 18696-18706, doi:10.1021/jp205477q (2011).
- 558 7 Frankel, G. S. *et al.* A comparative review of the aqueous corrosion of glasses, crystalline
559 ceramics, and metals. *npj Materials Degradation* **2**, 15, doi:10.1038/s41529-018-0037-2
560 (2018).
- 561 8 Gin, S. *et al.* Origin and consequences of silicate glass passivation by surface layers. *Nat*
562 *Commun* **6**, doi:Artn 6360
563 10.1038/Ncomms7360 (2015).
- 564 9 Rebiscoul, D. *et al.* Morphological evolution of alteration layers formed during nuclear glass
565 alteration: new evidence of a gel as a diffusive barrier. *J Nucl Mater* **326**, 9-18,
566 doi:10.1016/j.jnucmat.2003.10.015 (2004).
- 567 10 Collin, M. *et al.* Structure of International Simple Glass and properties of passivating layer
568 formed in circumneutral pH conditions. *npj Materials Degradation* **2**, 4, doi:10.1038/s41529-
569 017-0025-y (2018).
- 570 11 Munier, I., Crovisier, J. L., Grambow, B., Fritz, B. & Clement, A. Modelling the alteration gel
571 composition of simplified borosilicate glasses by precipitation of an ideal solid solution in
572 equilibrium with the leachant. *J Nucl Mater* **324**, 97-115, doi:10.1016/j.jnucmat.2003.08.033
573 (2004).
- 574 12 Hellmann, R. *et al.* Unifying natural and laboratory chemical weathering with interfacial
575 dissolution–reprecipitation: a study based on the nanometer-scale chemistry of fluid–silicate
576 interfaces. *Chem Geol* **294**, 203-216 (2012).
- 577 13 Gin, S. *et al.* Dynamics of self-reorganization explains passivation of silicate glasses. *Nat*
578 *Commun* **9**, doi:Artn 2169
579 10.1038/S41467-018-04511-2 (2018).
- 580 14 Cailleateau, C., Devreux, F., Spalla, O., Angeli, F. & Gin, S. Why Do Certain Glasses with a High
581 Dissolution Rate Undergo a Low Degree of Corrosion? *J Phys Chem C* **115**, 5846-5855,
582 doi:10.1021/jp111458f (2011).
- 583 15 Du, T. *et al.* Atomistic origin of the passivation effect in hydrated silicate glasses. *npj*
584 *Materials Degradation* **3**, 6, doi:10.1038/s41529-019-0070-9 (2019).

- 585 16 Gin, S., Beaudoux, X., Angeli, F., Jegou, C. & Godon, N. Effect of composition on the short-
586 term and long-term dissolution rates of ten borosilicate glasses of increasing complexity from
587 3 to 30 oxides. *J Non-Cryst Solids* **358**, 2559-2570, doi:10.1016/j.jnoncrysol.2012.05.024
588 (2012).
- 589 17 Fournier, M. *et al.* Effect of pH on the stability of passivating gel layers formed on
590 International Simple Glass. *J Nucl Mater* **524**, 21-38, doi:10.1016/j.jnucmat.2019.06.029
591 (2019).
- 592 18 Arena, H. *et al.* Impact of Zn, Mg, Ni and Co elements on glass alteration: Additive effects. *J*
593 *Nucl Mater* **470**, 55-67, doi:10.1016/j.jnucmat.2015.11.050 (2016).
- 594 19 Guo, X. L. *et al.* Self-accelerated corrosion of nuclear waste forms at material interfaces. *Nat*
595 *Mater* **19**, 310-+, doi:10.1038/s41563-019-0579-x (2020).
- 596 20 Collin, M., Fournier, M., Charpentier, T., Moskura, M. & Gin, S. Impact of alkali on the
597 passivation of silicate glass. *npj Materials Degradation* **2**, 16, doi:10.1038/s41529-018-0036-3
598 (2018).
- 599 21 Chave, T., Frugier, P., Gin, S. & Ayrat, A. Glass-water interphase reactivity with calcium rich
600 solutions. *Geochim Cosmochim Acta* **75**, 4125-4139, doi:10.1016/j.gca.2011.05.005 (2011).
- 601 22 Mercado-Depierre, S., Angeli, F., Frizon, F. & Gin, S. Antagonist effects of calcium on
602 borosilicate glass alteration. *J Nucl Mater* **441**, 402-410, doi:10.1016/j.jnucmat.2013.06.023
603 (2013).
- 604 23 Tribet, M. *et al.* New Insights about the Importance of the Alteration Layer/Glass Interface. *J*
605 *Phys Chem C* **124**, 10032-10044, doi:10.1021/acs.jpcc.0c02121 (2020).
- 606 24 Reiser, J. T. *et al.* Comparative structural investigations of nuclear waste glass alteration
607 layers and sol-gel synthesized aerogels. *npj Materials Degradation* **4**, 5, doi:10.1038/s41529-
608 020-0109-y (2020).
- 609 25 Kerisit, S., Pierce, E. M. & Ryan, J. V. Monte Carlo simulations of coupled diffusion and
610 surface reactions during the aqueous corrosion of borosilicate glasses. *J Non-Cryst Solids* **408**,
611 142-149, doi:10.1016/j.jnoncrysol.2014.07.020 (2015).
- 612 26 Hopf, J. *et al.* Glass-water interaction: Effect of high-valence cations on glass structure and
613 chemical durability. *Geochim Cosmochim Acta* **181**, 54-71, doi:10.1016/j.gca.2016.02.023
614 (2016).
- 615 27 Gin, S. *et al.* A General Mechanism for Gel Layer Formation on Borosilicate Glass under
616 Aqueous Corrosion. *J Phys Chem C* **124**, 5132-5144, doi:10.1021/acs.jpcc.9b10491 (2020).
- 617 28 Du, J. in *Molecular Dynamics Simulations of Disordered Materials: From Network Glasses to*
618 *Phase-Change Memory Alloys* (eds Carlo Massobrio, Jincheng Du, Marco Bernasconi, &
619 Philip S. Salmon) 157-180 (Springer International Publishing, 2015).
- 620 29 Deng, L. & Du, J. C. Development of effective empirical potentials for molecular dynamics
621 simulations of the structures and properties of boroaluminosilicate glasses. *J Non-Cryst Solids*
622 **453**, 177-194, doi:10.1016/j.jnoncrysol.2016.09.021 (2016).
- 623 30 Ha, M.-T. & Garofalini, S. H. Local structure of network modifier to network former ions in
624 soda-lime alumino-borosilicate glasses. *J Am Ceram Soc* **100**, 563-573,
625 doi:10.1111/jace.14565 (2017).
- 626 31 Ohkubo, T., Gin, S., Collin, M. & Iwadate, Y. Molecular Dynamics Simulation of Water
627 Confinement in Disordered Aluminosilicate Subnanopores. *Sci Rep-Uk* **8**, doi:Artn 3761
628 10.1038/S41598-018-22015-3 (2018).
- 629 32 Rimsza, J. M. & Du, J. Nanoporous silica gel structures and evolution from reactive force field-
630 based molecular dynamics simulations. *npj Materials Degradation* **2**, 18,
631 doi:10.1038/s41529-018-0039-0 (2018).
- 632 33 Collin, M. *et al.* Molecular Dynamics Simulations of Water Structure and Diffusion in a 1 nm
633 Diameter Silica Nanopore as a Function of Surface Charge and Alkali Metal Counterion
634 Identity. *J Phys Chem C* **122**, 17764-17776, doi:10.1021/acs.jpcc.8b03902 (2018).

635 34 Miyoshi, H., Hata, N. & Kikkawa, T. Theoretical Investigation into Effects of Pore Size and Pore
636 Position Distributions on Dielectric Constant and Elastic Modulus of Two-Dimensional
637 Periodic Porous Silica Films. *Japanese Journal of Applied Physics* **44**, 1166-1168,
638 doi:10.1143/jjap.44.1166 (2005).

639 35 Beckers, J. V. L. & de Leeuw, S. W. Molecular dynamics simulation of nanoporous silica. *J*
640 *Non-Cryst Solids* **261**, 87-100, doi:Doi 10.1016/S0022-3093(99)00607-9 (2000).

641 36 Rimsza, J. M. & Du, J. C. Structural and Mechanical Properties of Nanoporous Silica. *J Am*
642 *Ceram Soc* **97**, 772-781, doi:10.1111/jace.12707 (2014).

643 37 Nakano, A., Bi, L. S., Kalia, R. K. & Vashishta, P. Molecular-Dynamics Study of the Structural
644 Correlation of Porous Silica with Use of a Parallel Computer. *Phys Rev B* **49**, 9441-9452,
645 doi:DOI 10.1103/PhysRevB.49.9441 (1994).

646 38 Angeli, F., Gaillard, M., Jollivet, P. & Charpentier, T. Influence of glass composition and
647 alteration solution on leached silicate glass structure: A solid-state NMR investigation.
648 *Geochim Cosmochim Acta* **70**, 2577-2590, doi:10.1016/j.gca.2006.02.023 (2006).

649 39 Fluegel, A. Global model for calculating room-temperature glass density from the
650 composition. *J Am Ceram Soc* **90**, 2622-2625, doi:10.1111/j.1551-2916.2007.01751.x (2007).

651 40 Jégou, C. *Mise en évidence expérimentale des mécanismes limitant l'altération du verre R7T7*
652 *en milieu aqueux. Critique et proposition d'évolution du formalisme cinétique*, (1998).

653 41 Plimpton, S. Fast Parallel Algorithms for Short-Range Molecular-Dynamics. *J Comput Phys*
654 **117**, 1-19, doi:DOI 10.1006/jcph.1995.1039 (1995).

655 42 Le Roux, S. & Jund, P. Ring statistics analysis of topological networks: New approach and
656 application to amorphous GeS₂ and SiO₂ systems. *Comp Mater Sci* **49**, 70-83,
657 doi:10.1016/j.commatsci.2010.04.023 (2010).

658 43 Bhattacharya, S. & Gubbins, K. E. Fast method for computing pore size distributions of model
659 materials. *Langmuir* **22**, 7726-7731, doi:10.1021/la052651k (2006).

660 44 Pedone, A. Recent Advances in Solid-State NMR Computational Spectroscopy: The Case of
661 Alumino-Silicate Glasses. *Int J Quantum Chem* **116**, 1520-1531, doi:10.1002/qua.25134
662 (2016).

663 45 Atila, A., Ghardi, E., Hasnaoui, A. & Ouaskit, S. Alumina effect on the structure and properties
664 of calcium aluminosilicate in the percalcic region: A molecular dynamics investigation. *J Non-*
665 *Cryst Solids* **525**, doi:ARTN 119470
10.1016/j.jnoncrysol.2019.119470 (2019).

666 46 Bouhadja, M., Jakse, N. & Pasturel, A. Striking role of non-bridging oxygen on glass transition
667 temperature of calcium aluminosilicate glass-formers. *J Chem Phys* **140**, doi:Artn 234507
10.1063/1.4882283 (2014).

669 47 Benoit, M., Ispas, S. & Tuckerman, M. E. Structural properties of molten silicates from ab
670 initio molecular-dynamics simulations: Comparison between CaO-Al₂O₃-SiO₂ and SiO₂. *Phys*
671 *Rev B* **64**, doi:Artn 224205
10.1103/Physrevb.64.224205 (2001).

673 48 Allwardt, J. R., Lee, S. K. & Stebbins, J. F. Bonding preferences of non-bridging O atoms:
674 Evidence from O-17 MAS and 3QMAS NMR on calcium aluminate and low-silica Ca-
675 aluminosilicate glasses. *Am Mineral* **88**, 949-954, doi:Doi 10.2138/Am-2003-0701 (2003).

676 49 Delaye, J.-M. *et al.* Investigation of alumino-silicate glasses by coupling experiments and
677 simulations: Part I - Structures. *Manuscript submitted for publication* (2020).

678

679

680